Diversity through similarity: a world of polymorphs, solid solutions, cocrystals in a vial of 4,4'-diazopyridine

Diversity through similarity: a world of polymorphs, solid solutions, cocrystals in a vial of 4,4′-diazopyridine

*Paolo P. Mazzeo [1,2], Claudia Carraro [1], Anthea Arns [1†], Paolo Pelagatti [1,3], Alessia Bacchi [1,2]**

1 Dipartimento di Scienze Chimiche, della Vita e della Sostenibilità Ambientale, Università degli Studi di Parma, Viale delle Scienze, 17A, 43124 Parma, Italy. 2 Biopharmanet-TEC, Università degli Studi di Parma, Parco Area delle Scienze 27/A, 43124 Parma, Italy. 3 Centro Interuniveristario di Reattività Chimica e Catalisi (CIRCC), Via Celso Ulpiani 27, 70126 Bari, Italy.

KEYWORDS co-crystals, azopyridine, solid solutions, crystal engineering, polymorphism

ABSTRACT 4,4'-diazopiridine (AP) is largely known for its photophysical properties and it is extensively studied in solution as molecular switch. By contrast, AP is not similarly explored in the solid state. We here discuss the fine crystallographic interpretation of the electron density maps combined with occupancy refinement of solid solutions, cocrystals and solid solution of cocrystals of AP and some halogenated derivatives, obtained as a result of recrystallization experiments. AP halogenated derivatives are contained as impurities in the purchased starting material, and present a remarkable propensity to give cocrystals or solid solutions along with AP.

A new AP polymorph (**AP2**) has also been identified and phase evolution as function of temperature investigated by DSC and VT-XRPD.

Introduction

"You can see a lot just by observing" [1] – Joel Bernstein (1941-2019) loved to cite this famous quote by the baseball Hall-of-Famer Yogi Berra to remind researchers that visual observation of facts is the primary tool for scientific discovery. This paper reports how we discovered a whole crystallographic cave of wonders by careful visual inspection and wise crystallographic sense. We here describe an amazing family of conformational and packing behaviours displayed by 4,4′-diazopyridine (hereinafter referred as azopyridine, AP) and some halogenated derivatives (Scheme 1).

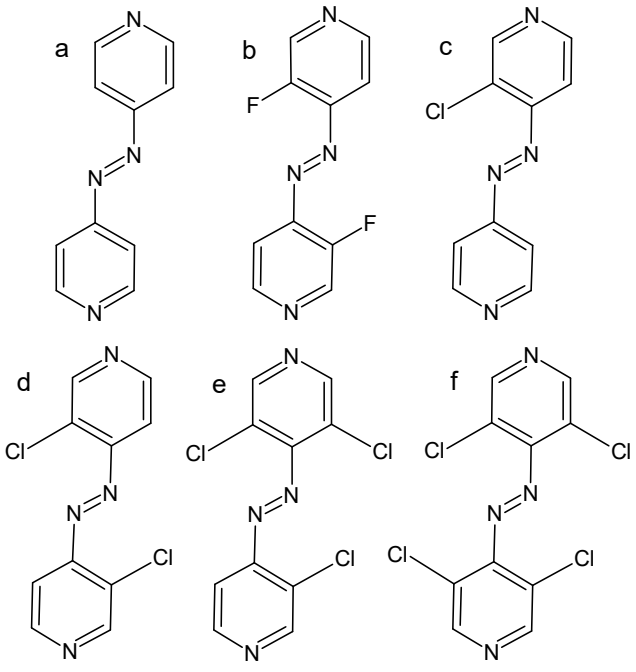

Scheme 1. Chemical sketches of the 4-4'diazopyridine (AP) (a) and its meta-substituted halogenated derivatives. (b) 3,3'-difluoro-4,4'diazopyridine (F_2AP), (c) 3-chloro-

4,4’diazopyridine (ClAP), (d) 3,3’-dichloro-4,4’diazopyridine (Cl_2AP), (e) 3,5,3’-trichloro-4,4’diazopyridine (Cl_3AP), (f) 3,5,3’,5’-tetrachloro-4,4’diazopyridine (Cl_4AP)

In the course of cocrystallization experiments of AP with natural products, which are reported elsewhere, we isolated a variety of crystals deriving, as we later realized, from the interactions of AP with some of its halogenated derivatives contained as impurities in the purchased starting material. Crystallization is conventionally regarded as the method of choice to purify a compound, as crystal nucleation and growth are extremely precise processes of supramolecular recognition. [2] However, crystallization from a mixture can equally well produce multicomponent crystals, such as solvates [3–5], cocrystals [6–14], or solid solutions [15–17], depending on the competition between homo-molecular and hetero-molecular interactions. Solvates and co-crystals are stoichiometric assemblies of two or more molecular components (at least one of which classified as a solvent in the case of solvates), where each component has a specific role in the crystal packing. By contrast, the stoichiometry of solid solutions is not limited to a single integer value but can be varied in continuum, and molecular components can substitute each other in the crystal packing.

In this work we describe solid solutions, cocrystals, and solid solution of cocrystals of AP with its halogenated derivatives F_2AP, Cl_2AP and Cl_4AP (Scheme 1).

Experimental

The crystal forms described in this paper were obtained during experiments aimed to co-crystallize AP with eugenol, a liquid natural oil with interesting antibacterial properties. [18]

Materials: 4,4’-diazopyridine was purchased from SigmaAldrich (88% purity) and used without further purification. Solvents used for crystallizations were used as purchased.

Synthetic procedures: a new polymorph of AP, **AP2**, was obtained by re-crystallization of the starting material by slow evaporation of MeOH in the presence of eugenol. After a few days, tiny needle-like orange crystals of the titled compound appeared. From the same crystallization batch, small plate-like crystals of **1** were concomitantly observed. **2** and **3** were concomitantly obtained by re-crystallization of the starting material by slow evaporation of DMSO in the presence of eugenol. Unexpectedly **1**, **2** and **3** resulted to be solid forms containing AP and its chlorinated derivatives present as impurities in the starting materials. **AP2** was also obtained as larger needle-like crystals from the melt: during the VT-XRPD analysis, larger crystals of both **AP1** and **AP2** polymorphs were concomitantly obtained once the sample was gradually cooled at 10°C/min from the melting to the ambient temperature.

Single Crystal Structure Determination: SC-XRD analyses were performed on single crystal samples by mean of a Bruker D8 Venture diffractometer equipped with a kappa goniometer. Low temperature data collections were performed under nitrogen flux by mean of an Oxford cryo-stream. Microfocused MoKα radiation (λ = 0.71073 Å) was used for all data collections; Lorentz polarization and absorption correction were applied. Data were reprocessed using Bruker APEX v3 software. Structures were solved by direct methods using SHELXT [19] and refined by full-matrix least-squares on all F^2 using SHELXL [20] implemented in Olex2-1.2. [21] For all structures anisotropic displacement parameters were refined except for hydrogen atoms. Crystal data for the compounds isolated in this work are reported in Table 1; details of the structural redetermination of **AP2** at RT and at 150 K are reported in the Supporting Information. ORTEP diagrams of all the compounds here characterized are reported in the Supporting Information. Crystallographic data for structures **AP2** (150K, 190K and 273K), **2-4** have been deposited with the CCDC 1938404-1938409 refcodes.

Energy calculations: intermolecular interactions were calculated by using the CE- B3LYP method [22] provided with CrystalExplorer [23]; energy frameworks were built with CrystalExplorer at the B3LYP/6-31G(d,p) level of theory [24]; lattice energies were calculated with the CE-B3LYP procedure in Crystal Explorer. [25]

Conformational Energy calculation: Conformational energy for Cl_4AP was calculated by using the Gaussian16 package [26] with the B3LYP [24] functional level in combination with the 6-311++g(d,p) basis set using Grimme's D3 [27] correction scheme for dispersion. The relaxed scan ranged from 0 to 180° by 5° intervals. [27–29]

Thermal analyses: Differential scanning calorimetry analysis of commercial AP were performed with a PerkinElmer Diamond equipped with a model ULSP 90 ultracooler. Heating was carried out in closed 10µl Al-pans at 5 °C/min in the temperature range −60 to 100 °C. The measurement was performed at atmospheric pressure under a constant flow of nitrogen (20 µl min^{-1}). The enthalpy of the endothermic or exothermic events was determined by the integration of the area under the differential scanning calorimetry (DSC) peak, which is reported in J/g (see Supporting Information).

Powder diffraction: X-ray Powder Diffraction (XRPD) data of commercial AP were collected in Bragg-Brentano geometry with CuKα radiation on a Rigaku Smartlab XE diffractometer equipped with a solid-state Hypix3000 2D detector. In order to increase the LoD of any crystalline impurity, data were collected with 5° soller slits and variable vertical slits which guarantees the same volume of sample under the beam along the measurement. Data were normalized to the counting time. The X-ray powder pattern collected at ambient conditions on commercial AP showed that **AP1** is the main crystalline phase, contaminated by the chlorine containing phase **1**. Additional extra peaks related to phase **2** (minority phase) were also

observed. No Bragg peaks related to Cl_3AP or Cl_4AP were observed due to their low concentration in the raw material (see Supporting Information). In-situ non-ambient temperature XRPD data were collected on the same instrument equipped with an Anton-Paar TTK600 non-ambient chamber with flat sample holder suitable for BB geometry. A comparable thermal profile as used for DSC analysis was applied: temperature was increased in step from 25°C to 110 °C at 5°C min^{-1}, data collections were performed while holding the sample at a given temperature. Thermal scheme as well as fine phase evolution interpretation are reported in the Supporting Information.

Spectrometric detection of halogenated side products: DIP-MS-EI(-) analysis was conducted by means of a Thermo Fisher DSQII single quadrupole spectrometer, equipped with a DIP (Direct Insertion Probe) for the direct analysis of solid samples. The EI spectra were acquired at 70eV in negative mode. The source temperature was 200 °C while the probe temperature was 70°C. The following m/z signals were observed: m/z = 184 $[C_{10}H_8N_4]^-$, m/z = 218 $[C_{10}H7ClN_4]^-$, m/z = 252 $[C_{10}H_6Cl_2N_4]^-$, m/z = 286 $[C_{10}H_5Cl_3N_4]^-$, m/z = 322 $[C_{10}H_4Cl_4N_4]^-$. All the signals were in agreement with the expected isotopic patterns (see Supporting Information). No signal of the fluorinated derivative was observed, likely due to its extremely low concentration.

Results and discussion

The crystal structure of AP is already reported in the literature as a *P-1* triclinic form, **AP1**, with data experimentally determined at RT and at 190 K, respectively. [30] The form **AP1** had been crystallized from a saturated solution of 5: 1: 1 hexane: EtOH: toluene (v/v/v), whilst our new form **AP2** was crystallized from MeOH in the presence of eugenol. The crystal structure was

determined at RT even though crystals of the same phase were also obtained by cooling from the melt and the same structure was then redetermined at 150 K and 190 K.

Table 1 Crystal data and structure refinement for **AP2@190K**, **1**, **2** and **3**

Compound Name	**AP2**	**1**	**2**	**3**
Empirical formula	$C_{10}H_{7.89}F_{0.11}N_4$	$C_{10}H_{7.14}Cl_{0.85}N_4$	$C_{20}H_{12}Cl_4N_8$	$C_{20}H_{12.63}Cl_{3.51}N_8$
Formula weight	186.09	213.47	506.18	489.43
Temperature/K	190	190	200	150
Crystal system	monoclinic	monoclinic	monoclinic	monoclinic
Space group	$P2_1/n$	$P2_1/n$	$P2_1/n$	$P2_1/n$
a/Å	4.7801(5)	21.33(4)	11.869(3)	13.796(5)
b/Å	6.2275(6)	6.10(1)	5.3884(8)	3.9715(7)
c/Å	15.4171(16)	3.826(7)	16.7621(19)	19.328(3)
α/°	90	90	90	90
β/°	96.133(3)	96.72(4)	97.234(4)	103.082(5)
γ/°	90	90	90	90
Volume/Å^3	456.31(8)	494.4(16)	1063.5(3)	1031.6(5)
Z	2	2	2	2
ρ_{calc}g/cm^3	1.354	1.434	1.581	1.576
μ/mm^{-1}	0.089	0.313	0.584	0.538
F(000)	194.0	219.0	512.0	497.0
Crystal size/mm^3	0.08 × 0.05 × 0.04	0.07 × 0.04 × 0.04	0.04 × 0.03 × 0.02	0.05 × 0.04 × 0.04
Radiation/Å	MoKα (λ = 0.71073)	MoKα (λ = 0.71073)	MoKα (λ = 0.71073)	MoKα (λ = 0.71073)
2Θ range for data collection/°	7.062 to 51.486	6.952 to 39.508	4.484 to 54.198	6.064 to 41.716
Reflections collected	10136	4732	9618	3857
Independent reflections	874 R_{int} = 0.0233 R_{sigma} = 0.0102	440 R_{int} = 0.1155, R_{sigma} = 0.0581	2343 R_{int} = 0.1298 R_{sigma} = 0.1400	1042 R_{int} = 0.0409 R_{sigma} = 0.0442
Data/restraints/parameters	874/0/74	440/457/124	2343/3/163	1042/18/155
Goodness-of-fit on F^2	1.085	1.214	0.961	1.185
Final R indexes [I>=2σ (I)]	R_1 = 0.0366 wR_2 = 0.0944	R_1 = 0.1218 wR_2 = 0.2734	R_1 = 0.0619 wR_2 = 0.1330	R_1 = 0.0779 wR_2 = 0.1660
Final R indexes [all data]	R_1 = 0.0389 wR_2 = 0.0961	R_1 = 0.1373 wR_2 = 0.2836	R_1 = 0.2090 wR_2 = 0.1974	R_1 = 0.0906 wR_2 = 0.1722
Largest ΔF max/min / e Å^{-3}	0.14/-0.18	0.41/-0.31	0.34/-0.33	0.51/-0.52

Compound **AP2** crystallizes in the monoclinic *P2₁/n* space group, and the molecules are planar and sit on inversion centers located in the middle of the N=N bond. Energy frameworks calculated by CrystalExplorer[23] at the B3LYP/6-31G(d,p) theory level for the structure determined at 190K were used to analyze the packing stabilization compared to the already

known polymorph **AP1** determined at 190K [CSD refcode: EVESIJ04 [30]]. Contrarily to what one would expect by simple analysis of intermolecular distances, which evidences short C-H…N contacts, the main contribution to the packing energy refers to dispersion terms. In **AP2**@190K molecules are arranged in stacked pillars (interplanar distance = 3.413 Å, offset= 3.39 Å), where the intermolecular stabilization (A…B, E=-27.3 kJ/mol) has mainly dispersive nature (Figure 1 – for the energy decomposition see Supplementary Information); **AP1**@190K has a slightly larger but less offset stacking arrangement (interplanar distance 3.541 Å, offset 1.48 Å) and similar intermolecular A…B stabilization (E=-30.2 kJ/mol). The second most important contribution to the packing refers to hydrogen bonds: in **AP2**@190K the pillars are arranged in a 2D grid based on C-H..N contacts (A…C/E, E=-13.0 kJ/mol) with a strong coulombic stabilization between pyridinic nitrogen and CH of two adjacent molecules C and E (C-H…N(i) 3.420(1) Å, 149(2)°, i = $^1/_2 - x$, $^1/_2 - y$, $^3/_2 - z$) and a substantially dispersive interaction (E=-11.7 kJ/mol) between coplanar parallel molecules (A…D)/(C…E). Similar interactions are observed in the polymorph **AP1**@190K, (E(A…C)=-15.5 kJ/mol, E(A…E)= -15.3 kJ/mol), with a weaker A…D contribution E(A…D)=-6.1kJ/mol), compensated by a significant dispersive B…D interaction (-18.4 kJ/mol). In **AP2** consecutive molecules A, C alternate the orientation of the N=N bond by means of a screw axis within the 2D layer, while in **AP1** they are all parallel and related by simple translation. Interestingly, this layered arrangement causes a loose packing between molecules in the layers (Figure 1) reflected in the lower stabilization of the molecular pair A…D than A…C within the 2D grid evidenced by the energy frameworks calculations. By carefully analyzing the final electron density map of **AP2**@190K (Figure 2), we detected the possibility that this feature of the crystal packing induces the formation of a solid solution of AP with an impurity present in the commercial product. In fact, the final electron density difference map for

compound **AP2**@190K showed a clear residual electron density at a distance of 1.38 Å to one of the carbon atoms in meta position (Figure 2), with a maximum residual density of about 0.7 e/Å^3. The distance suggested the possible partial presence of a mono meta-fluorinated species. After modeling the residual peak as a fluorine atom with 5% occupancy, the final map was featureless (min: -0.2 max: 0.2 e/Å^3) and the R_1 factor dropped from 5.05 to 3.66%. Redetermination of the crystal structure at 150 K gave identical results for **AP2**@150K, while redetermination at RT on a different crystal gave a slightly higher occupancy for the fluorinated specie in **AP2**@RT (see Supplementary Information).

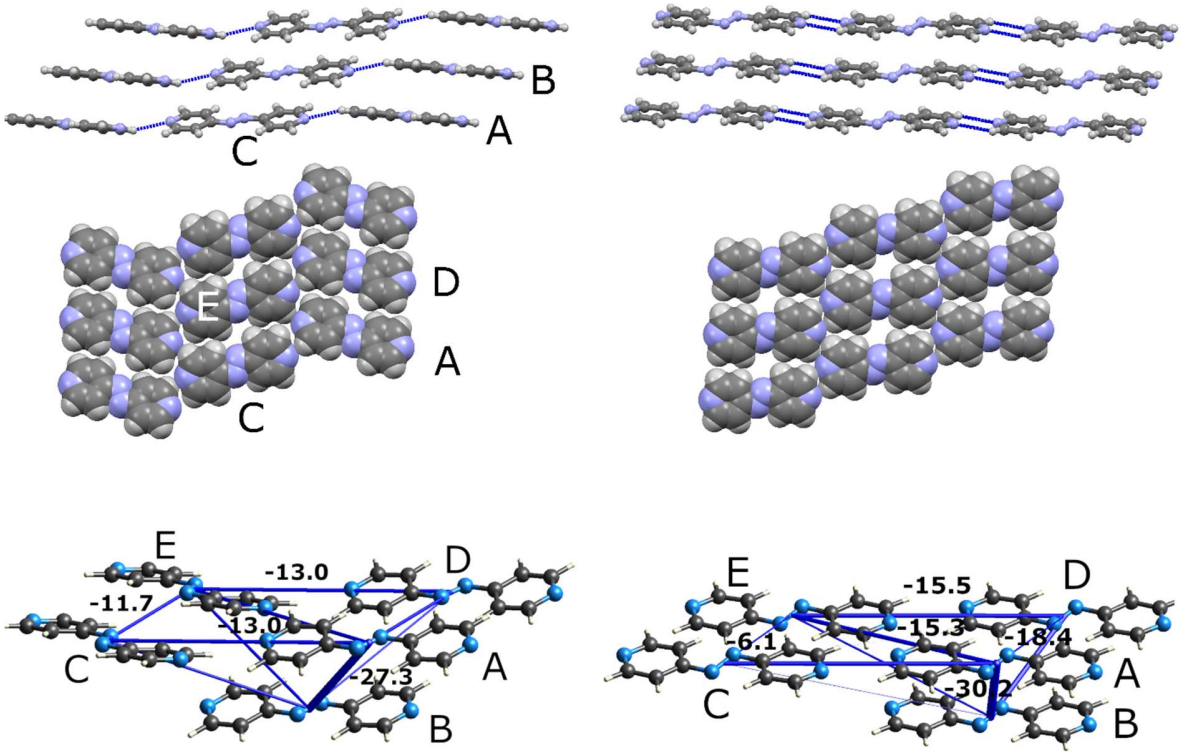

Figure 1. Top: Main interactions between molecular pairs in **AP2**@190K (left) and **AP1**@190K (right). Middle: Comparison of the layer arrangement of **AP2** (left) and **AP1** (right). Bottom:

energy frameworks for **AP2** (left) and **AP1** (right) (kJ/mol). A…B = stacking interactions, A…C/A…E/D…E = CH…N hydrogen bonds (dotted), A…D/C…E = dispersive interactions.

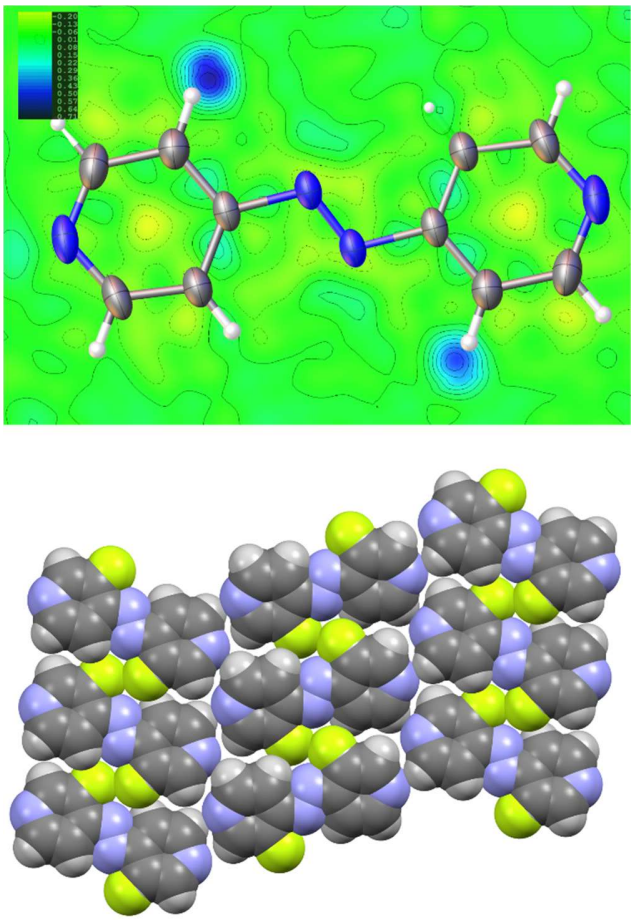

Figure 2. Top: Residual electron density for **AP2**@190K when modelled without fluorine impurities, min: -0.20 max: 0.7 e/Å^3. Bottom: crystal packing of **AP2** evidencing the position of the 5% occupied fluorine atoms.

To verify if the same phenomenon was present also in **AP1**, we repeated the refinement of **AP1** with the original literature data by taking advantage of the deposited structure factors in the CSD [30], and found a flat map. Therefore, it is not the contamination of a small percentage of the meta-fluorinated species which induces the apparent loose packing, but conversely it is the loose packing which allows the incorporation of a suitable impurity in the crystal of **AP2**. **AP2** may be

considered a solid solution between the **AP2** polymorph of azopyridine, and the F_2AP derivative. Full energy frameworks for the two forms **AP1**@190K and **AP2**@190K are compared in the Supporting Information, showing a remarkable similarity.

Although at present we cannot explain the presence of fluorinated impurity, this seems to have a stabilizing effect on the stacking dispersive interactions, which increase significantly to E = -34.3 kJ/mol (in the limiting hypothesis of a contact between two fluorinated molecules), while the other two main stabilizing factors remain practically the same (A…C = -12.9 kJ/mol, A…D = -8.1 kJ/mol, this one being weakened by the repulsive contribution among F atoms (Figure 2).

The total lattice energy of the two polymorphs **AP1** and **AP2** was estimated by CrystalExplorer at the B3LYP/6-31G(d,p) level of theory, by neglecting the occurrence of fluorinated impurities. Relaxation energy regarding conformational rearrangements was considered the same for both structures, since in both cases the azo molecule is planar. [31] Lattice energy for **AP2** results -97.3, -100.4, -109.0 kJ/mol respectively for RT, 190K and 150 K, contrasted with the values for **AP1**: -100.8 and -105.4 kJ/mol for RT and 190 K respectively. The differences point to **AP1** being the most stable form at 0 K, neglecting thermal expansion effects[32,33] and uncertainty of the computational method. [25] In order to check the relation between the two forms at ambient conditions, the system was investigated by DSC and VT-XRPD (*vide infra*).

Within the crystallization trials of **AP2** (see experimental), we were able to isolate chloride derivatives of azopyridine too, which present a remarkable propensity to give cocrystals or solid solutions. The chlorine-containing species were clearly detected in the commercial products by EI-MS analysis as the mono-, di- tri- and tetra-chloro derivatives (see Supporting Information). Solid solutions involving the replacement of drug molecules with their halogen-substituted

analogue have been reported in the literature and are ascribed to the similar molecular shape of the molecules involved. [34–37]

1 crystallizes in the monoclinic $P2_1/n$ space group. It actually consists of a solid solution of AP (57%) and Cl_2AP (43%), where Cl_2AP is further disordered over two orientations (Cl_2AP-a 37% and Cl_2AP-b 6% respectively) (Figure 3). This uncommon model was built by careful inspection of the electron difference map combined with occupancy refinement of the different components. In fact, the refinement of a single Cl_2AP molecule leads initially to having two orientations with chlorine atoms with refined occupancy of 37% and 6% respectively. This model leaves evident residuals of further positive residual density tracing a second molecule slightly displaced and a second partial chlorine atom (blue peaks in Figure 3), and negative electron density residuals (red) indicating a less than unitary occupation of the actual model.

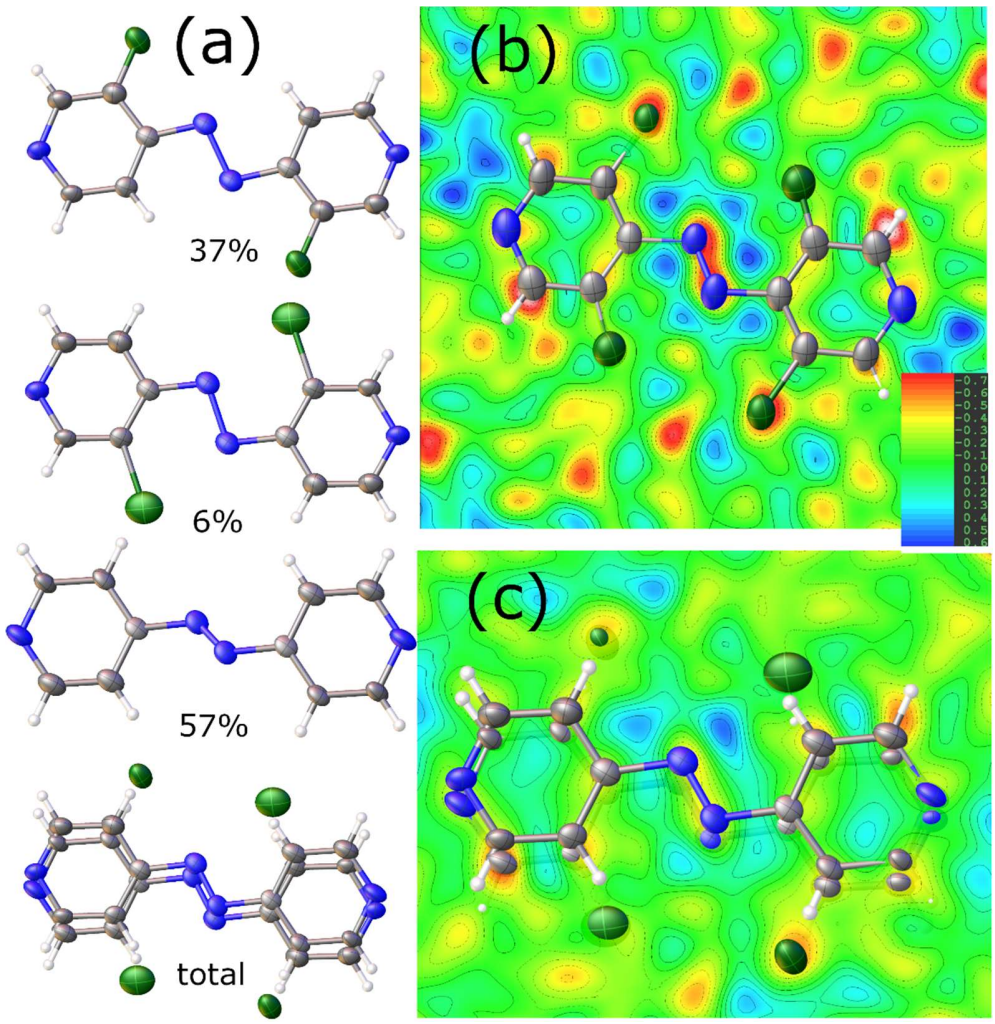

Figure 3. (a) Co-existence of three molecular entities in **1**, with refined occupancies, and overall final model (b) Difference electron density map (max/min= 0.7/-0.6 e/Å^3) obtained by refining a single Cl_2AP molecule, with chlorine atoms partially occupied (37% and 6%). Blue residuals reveal the presence of a second slightly displaced molecular component, which was successfully modeled as an AP molecule with 57% occupancy, while red residuals indicate that the occupancy must be lowered, hence Cl_2AP refined to 43% occupancy. (c) Final difference electron density map with (Cl_2AP-a 0.37: Cl_2AP-b 0.06: AP 0.57) composition.

Therefore, a second molecular entity was modeled, containing no chlorine atoms, and the complementary occupancy of the Cl_2AP and AP entities were refined. The R_1 factor reduced from 12.82 to 12.18% and the final difference electron density map was significantly improved (max/min= 0.7/-0.6 e/Å^3) (Figure 3).

Thus the structure of **1** consists of a solid solution of AP and Cl_2AP molecules, which pack with a pattern reminiscent of **AP2**, namely displaying a pillared stacking with 3.427 Å A…B interplanar distance, and short CH…N interactions between A…C pyridinic groups of different pillars (C-H…N C..N=3.486 (2) and 3.447(3) Å, C-H...N = 145 and 156° respectively) (Figure 4). Differently from **AP2**, in this case the contacts bridge molecule across the pillar, so that adjacent A, C molecules are not arranged in layers, but are tilted. Interestingly, the motif of parallel A…D coplanar molecules seen in **AP1** and **AP2** recurs also for Cl_2AP and accommodates the occasional steric hindrance of partially occupied chlorine atoms (Figure 4).

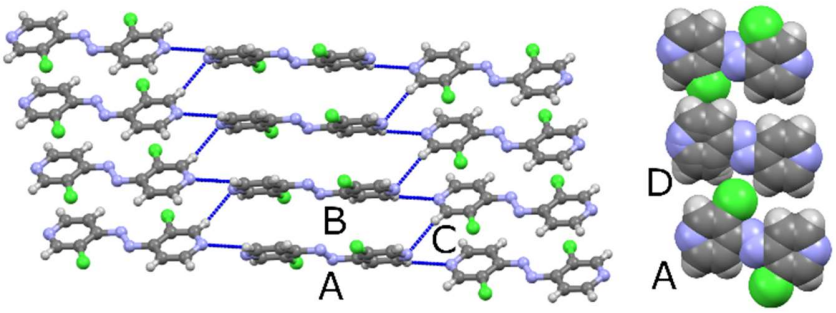

Figure 4. Left: Packing arrangement in **1**, evidencing the A…B stacking and the A…C C-H…N hydrogen bonds as observed for **AP1** and **AP2**, see Figure 1. Disorder has been omitted for clarity. Right: Example of array of parallel A (Cl_2AP) and D (AP) molecules for **1**, where the three molecular components of the solid solution are represented as an example.

From the crystallization experiment of commercial AP performed in DMSO (see experimental), other two crystalline compounds were isolated, which resulted to be two polymorphs of the 1:1 cocrystal between AP and Cl_4AP, namely **2** and **3**.

2 crystallizes in the monoclinic *P2₁/n* space group, where both components, AP and Cl_4AP are located on the inversion centers. The most striking structural features exhibited by **2** is the coplanarity of the four chlorine atoms of Cl_4AP (dihedral angle between pyridine rings = 0.0°), which intuitively would be expected to adopt a conformation less hindered by mutual repulsion; this is combined with the disorder of the N=N group of the Cl_4AP molecule over two alternate positions (Figure 5). From inspection of the difference electron density map after the last anisotropic refinement, in fact, it is clear from the residuals that the azo group in both molecules is disordered over two orientations (Figure 5). The disorder was modeled as 0.5/0.5 and 0.33/0.67 distribution for Cl_4AP and AP molecules respectively, the R_1 factor dropped from 10.1 to 6.2% with a featureless final map.

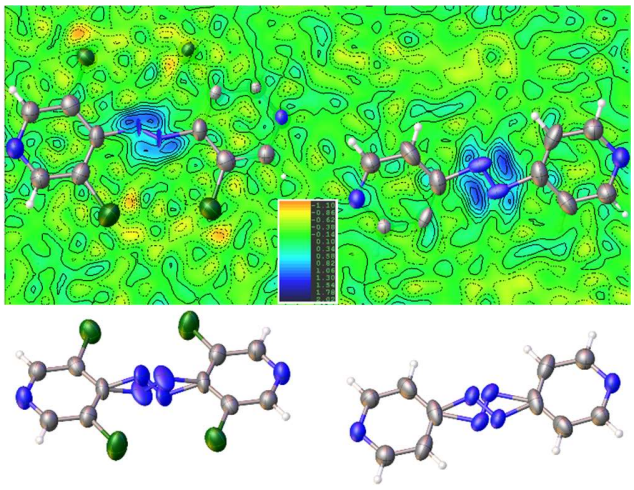

Figure 5. Difference electron density map for **2** evidencing peaks pointing at disorder of the azo group (maximum 2.0, minimum -0.6 e/Å^3), and refined model below.

The cause of the unexpected planarity of Cl_4AP was investigated by computational analysis. The conformational energy of the Cl_4AP molecule related to the reciprocal orientation of the pyridine groups and to the geometry of the N=N group has been calculated with Gaussian16 package[26] to understand if the two features are related, and if the counterintuitive coplanar arrangement of the four chlorine atoms may be favored by the packing stabilization. We explored the 180° rotation of the structure around the dihedral angle ϕ 7-1-12-13 (Figure 6). The relaxed scan shows that in the gas phase the solid-state geometry (**I**) is significantly different from the most stable form **III** (**I** ϕ = 13°; **III** ϕ = 83°). The energy difference between **III** and **I** is 5 kJ/mol, and it is due to a combination of repulsive and electronic effects. In fact, upon variation of ϕ we also observed a change in the length of N=N bond, and a concomitant flip of the azo bond, mirroring the disorder observed in the electron density map. Visualization of the HOMO orbital of **II** and **IV**, corresponding to minimum and maximum of N=N bond length respectively, shows that in **II** the N=N bond is shorter than in **IV** because the lone pairs (sp^2) of the nitrogen atoms are delocalized on the pyridine rings, thus decreasing the repulsive forces (see Supporting Information); conversely in **IV** the orbitals conjugated with the aromatics systems of pyridine are *p*-type (N=N double bond), resulting in a longer bond length as less electron density is delocalized on the aromatic system. Further variation in ϕ brings the structure abruptly back to conformation **II** (**V** ≡ **II** in the Figure 6).

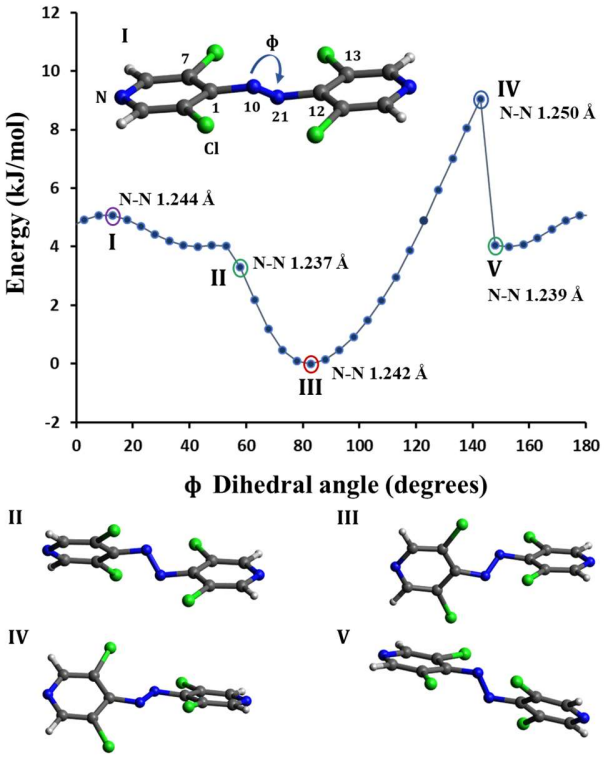

Figure 6. (top) Dependence of the gas phase energy of Cl_4AP on dihedral angle ϕ in **2**. Solid-state geometry relaxed in gas phase ϕ(**I**) = 12°. (down) Geometry of conformations along the scan: **II,** minimum N_{10}-N_{21}, ϕ = 57°; **III**, minimum energy, ϕ = 83°. **IV**, maximum energy in gas phase, maximum N_{10}-N_{21}, ϕ =142°; **V**, ϕ = 148°, azo group orientation and length is restored as in **II**.

In fact, the main stabilization factor in the packing of **2** is represented by the dispersive stacking of Cl_4AP molecules (-34.6 kJ/mol), as calculated by CrystalExplorer[23] at the B3LYP/6-31G(d,p) level of theory (Figure 7). This compensates the conformational expense required to flatten the molecule discussed in the previous paragraph. Within the stacked columns, Cl_4AP molecules are separated by an interplanar distance of 3.59 Å, and are significantly offset by 4.03 Å. AP molecules are also arranged in offset stacked pillars (E = -20.2 kJ/mol), with shorter

interplanar distance (3.21 Å) and larger offset (4.32 Å). The Cl_4AP and AP columns interact by C-H…N contacts (E = -16.4 kJ/mol, 3.401(2) Å, 146(2)°) forming slabs (Figure 7) exposing at the surface alternately pairs of Cl atoms oriented as a pincer, and N atoms of the azo groups. This arrangement supports the aggregation of the slabs (E=-12.2 kJ/mol) through the biting of the array of paired Cl atoms on the array of azo groups of an adjacent slab, by halogen bonding (Cl…N = 3.260(2) Å)) and long Cl…H-C contacts (H…Cl = 3.0-3.1 Å) creating an orthogonal reciprocal orientation (dihedral angle = 83°).

From the same crystallization batch of **2**, we obtained a second concomitant polymorph of the AP:Cl_4AP cocrystal, namely **3**, which also crystallizes in the monoclinic space group $P2_1/n$. The structure contains one AP molecule and one Cl_4AP molecule both located on the inversion centers. The analysis of the electron density on the chlorine atoms of Cl_4AP (Figure 8), however, suggests that they are not fully occupied, namely 80% and 88% respectively, indicating the presence of a mixture of Cl_4AP (up to 80%), Cl_2AP (up to 8%) and AP (12%) molecules on the same site. Moreover, the difference electron density map highlights a significant residual at chlorine bonding distance from the meta-carbon of the AP molecule (Figure 8), modeled as a partially occupied chlorine (6%). With this model of occupational disorder, the structure improves from R_1 = 9.30 to 7.79% and the final map is practically featureless. The final picture is therefore a AP:Cl_4AP cocrystal with partial substitution of Cl_2AP on both sites. As for **2**, **3** also exhibits perfect coplanarity of the four chlorine atoms of Cl_4AP, combined with the disorder of the azo group of the Cl_4AP molecule over two alternate positions (Figure 8). Energy framework calculations performed on the structure simplified as a 1:1 AP:Cl_4AP cocrystal (Figure 9) shows that the main packing stabilization is due to the stacking of segregated columns of Cl_4AP and AP, contributing by -47.9 and -28.8 kJ/mol respectively (Figure 9).

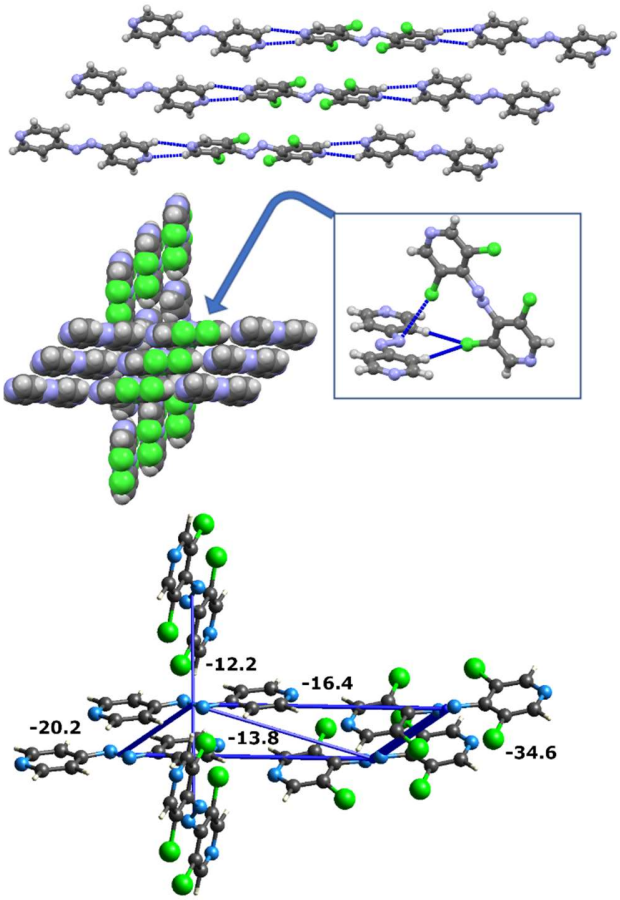

Figure 7. Top: slabs formed by stacked arrays of Cl_4AP and AP molecules, interacting by CH…N hydrogen bonds in **2**. Center: orthogonal arrangement of adjacent slabs, via biting of Cl on N (inset). Bottom: energy framework for **2** (kJ/mol), threshold -9 kJ/mol.

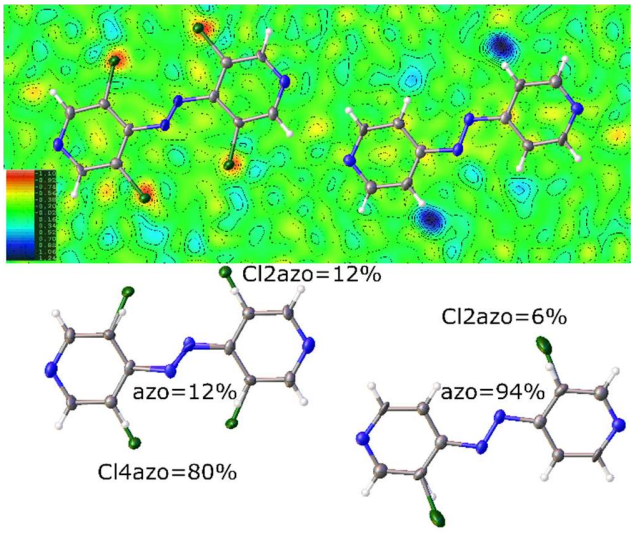

Figure 8. Difference electron density in **3**, when modelled as a 1:1 AP:Cl_4AP cocrystal, showing residuals corresponding to partially occupied chlorine atoms (max/min=1.24/-1.10 e/Å^3). The residual density was modeled as displayed in the bottom part, with Cl_4AP (up to 80%), Cl_2AP (up to 8%) and AP (12%) occupying one site, and AP (94%) and Cl_2AP(6%) the other site of the cocrystal.

The mainly dispersive attraction between planar Cl_4AP molecules largely compensates the conformational energy loss described above. Cl_4AP and AP molecules show a stacking distance of 3.46 Å and 3.40 Å respectively, and an offset of 1.9 Å and 2.0 Å respectively, being therefore much better piled than in **2**. A mainly coulombic stabilization between stacked arrays of AP and Cl_4AP is obtained by C-H…N (3.604(6) Å, 152(4)°) hydrogen bonds between pyridine rings (-15.9 kJ/mol), which originate slabs in the *bc* plane. As in **2**, these slabs are arranged in a tilted fashion and connected by N…Cl halogen bonds and C-H…Cl contacts (-10.0 kJ/mol). However, the tilt angle is lower than in **2** (63°).

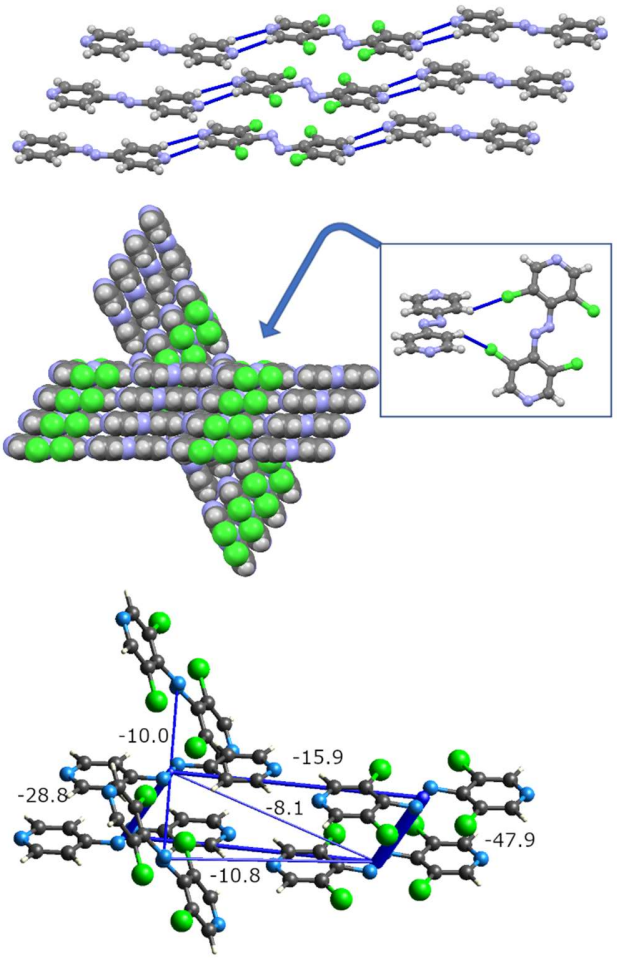

Figure 9. Packing of **3** (occupational disorder omitted). Top: slabs formed by stacked arrays of Cl_4AP and AP molecules, interacting by CH…N hydrogen bonds. Center: tilted arrangement of adjacent slabs, via biting of Cl on N (inset). Bottom: energy framework for **3**, threshold -9 kJ/mol.

The lattice energy of the two forms **2** and **3** have been estimated by using the procedure of CrystalExplorer[23] at the B3LYP/6-31G(d,p) level of theory, considering a fully ordered 1:1 occupancy of the two molecular partners in both structures. **3** resulted more stable than **2** (-112.7

and -109.5 kJ/mol, respectively). Full energy frameworks for the two forms are compared in the Supporting Information.

Phase evolution as function of temperature

DSC analysis performed on the commercial AP is reported in Figure 10 (inset). Two heating/cooling cycles were performed to test the reproducibility of the thermal events. Details are reported in the Supplementary Information. The fine phase interpretation is reported below in the VT-XRPD paragraph. An endothermic peak at 77°C related to the **AP1**-to-**AP2** phase transition is observed during the heating process (from 30°C to 100°C at 5 °C min^{-1}), then, at 96°C (broad peak), the melting of the sample occurred. The ΔH calculated for the first peak (12.20 J/g) is significantly lower than the one reported for the second peak (89.42 J/g) which is symptomatic of a non-complete **AP1**-to-**AP2** phase transition. The broad peak associated to the melting event actually suggests the presence of both **AP1** and **AP2** as well as other halogenated species, as confirmed by XRPD. During the cooling process (from 100 to -30 at 5°C min^{-1}), a series of exothermic events were observed: the main exothermic peak centered at 79°C is related to the multiple recrystallization of different species (*vide infra*) to which a **AP2**-to-**AP1** phase conversion follows at 62°C suggesting an enantiotropic relationship between the two AP polymorphs. During the second heating/cooling cycle, the samples undergoes the same endothermic/exothermic events: the broader peaks, compared with those observed in the first cycle, convey that the all the events are sensibly kinetically dominated.

Variable Temperature X-Ray Powder Diffraction (VT-XRPD) analysis performed in non-ambient conditions were performed on commercial AP (Figure 10) to better understand the phase evolution already observed by DSC as function of temperature. The sample was exposed to a firing profile consistent to the heating cycles used for the DSC analysis.

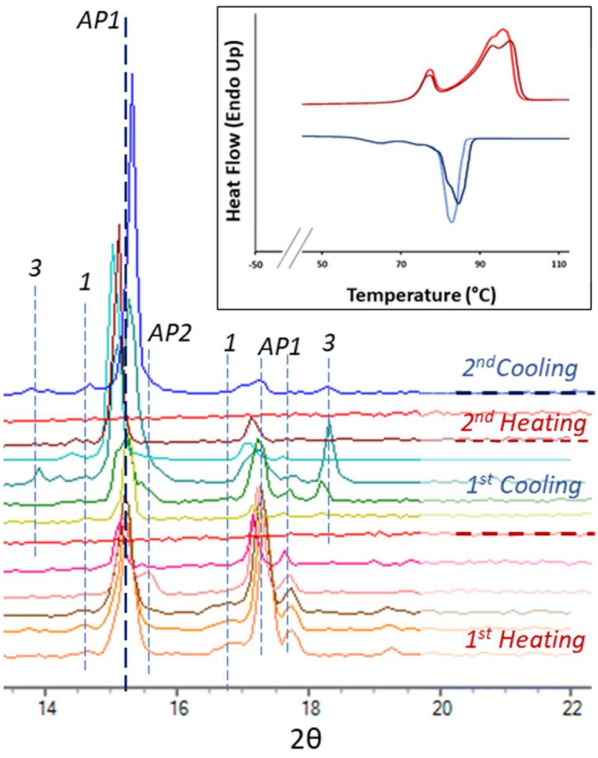

Figure 10. VT-XRPD analysis performed on AP starting material. Two heating/cooling cycles were performed in sequence on the same sample. The XRPD patterns are y-offset displayed and labelled accordingly. For the sake of clarity, the 2-theta values reported are limited to the range where only the most representative peaks for the phases under investigation (labelled accordingly in the picture) are observed. (inset) DSC thermal profile registered on the commercial AP. The temperature reported is only limited to the range where thermal events are registered. The two subsequentially heating/cooling cycles performed are represented with the following color code: 1st heating red, 1st cooling light blue, 2nd heating dark red, 2nd cooling dark blue.

The phase evolution interpretation at each temperature is reported in the Supporting Information. AP was heated from ambient temperature up to 100 °C at 5 °C/min and then cooled down to ambient temperature with the same thermal gradient. It is worth notice that **AP1** was the

major crystalline component in the as purchased sample, even though some extra peaks related to **1** and **2** were detected as impurity. The mixture remained stable up to 70°C when some extra peaks, related to the other polymorph **AP2**, came up. At 90°C the intensity of the peaks related to **1** decreased while the **AP2** increased significantly. At 95°C both **AP1** and **AP2** were present in the mixture. By increasing the temperature, the intensity of the Bragg peaks related to **AP2** decreased before those of **AP1** suggesting that the melting point of **AP2** is lower than that of **AP1**. After melting occurred at 100°C, the sample was cooled down to 60°C: at 90 °C both **AP2** and **AP1** crystallize. After recrystallization from the melt, the X-ray pattern is massively characterized by preferential orientation of **AP1** which could negatively influence the LoD of any additional phase (if any). It is worth notice that, after melting, also **1** and **3** crystallized on cooling the sample down at 75 °C. A second heating profile was performed up to the melting (100°C) at 5 °C/min. The same phase evolution was observed with the exception that the mixture was now composed by **AP1**, **AP2**, **1** and **3**. The broader peaks observed in DSC during the second heating profile is thus justified by the emergence of more side-structures with respect to those present in the raw material. As a confirmation that kinetic plays a key role in the formation of satellite crystalline phases as function of temperature, we quickly cooled the sample from the melt to 90°C unexpectedly showing that **3** is present as major component. After melting and cooling again the sample with no holding time from 100 °C to 25 °C we observed that **AP1** (massively preferentially oriented) and **AP2** are both present at room temperature. **2** and **3** are also present as satellite phases.

Conclusions

The findings of this work show how the presence of impurities in a crystallization batch can originate a landscape of structural variations, from solid solutions where the impurity are easily accommodated in the main crystal framework, to cocrystals where the unexpected guest plays a pivotal role in determining the crystal structure, to solid solutions of mixed partners where all the components can be accommodated. The important conclusion is that the final outcome depends on the molecular structure of the impurity.

In fact, comparison of **AP1** and **AP2** shows that AP is a flat, centrosymmetric molecule and it is propense to pack by organizing stacked pillars stabilized by strong dispersive interactions, which assemble by coulombic C-H…N contacts giving slabs which further associate by dispersive loose contacts. These loose contacts allow to incorporate fluorinated impurities in the structure, whose slightly augmented steric hindrance fits well in the small empty spaces of the **AP2** structure, giving a solid solution. Substitution of fluorine with the more abundant and sterically hindered chlorine impurity (Cl_2AP) leads to a significant tilt of the pillars within the slab, necessary to accommodate the bigger halogen, and, consequently, to the distortion of the structure. A dramatic change occurs when a Cl_4AP impurity shares the crystal packing with AP: like in **AP1**, **AP2** and **1**, both AP and Cl_4AP molecules are planar and strongly propense to pack in slabs made by stacked pillars connected by C-H…N interactions, as seen in **2** and **3**. However, the two faced meta-chlorine atoms on the same of Cl_4AP provide a strong supramolecular bite to interact with the azo group of AP, which strongly tilts the slabs. Two forms of tilting are observed, depending on the Cl_4AP content (**2** and **3**). The interplay between molecular structure and crystal packing is two-faced: on one hand the strong stacking stabilization forces Cl_4AP to adopt a flat conformation that, in turn, creates the supramolecular bite governing the assembly of the slabs. Molecules AP, F_2AP, Cl_2AP, Cl_4AP have similar shape and occur concomitantly in

commercial azopyridine, generating a variety of different crystalline arrangements based on a diverse combinations of intermolecular interactions.

ASSOCIATED CONTENT

Supporting information

The Supporting Information is available free of charge on the ACS Publications website at DOI: 10.1021/acs.cgd.xxxxxxx. Experimental section, summary of crystal data and refinement results and ORTEP pictures of **AP2** (RT, 150K and 190K), **1-3.** Summary of the DSC analysis, fine interpretation of the phase evolution as function of temperature (VT-XRPD) of AP, Energy Framework calculation and additional information about conformation analysis of Cl_4AP in **2** and **3** (PDF)

Accession Codes

CCDC 1938404-1938409 contain the supplementary crystallographic data for this paper. These data can be obtained free of charge via www.ccdc.cam.ac.uk/data_request/cif, or by emailing data_request@ccdc.cam.ac.uk, or by contacting The Cambridge Crystallographic Data Centre, 12 Union Road, Cambridge CB2 1EZ, UK; fax: +44 1223 336033.

AUTHOR INFORMATION

Corresponding Author

* Alessia Bacchi, Dipartimento SCVSA, University of Parma, Viale delle Scienze 17/A, 43124 Parma, Italy. alessia.bacchi@unipr.it.

Present Addresses

† AA, Institut fuer Anorganische und Analytische Chemie, J. W. Goethe Universitaet, Frankfurt am Main, Frankfurt am Main, Germany

Author Contributions

The manuscript was written through contributions of all authors. All authors have given approval to the final version of the manuscript.

Funding Sources

Project funded by the MIPAAFT (Ministero delle Politiche Agricole Alimentari , Forestali e del Turismo), “Bando per progetti innovativi contro gli sprechi e per la gestione delle eccedenze alimentari” – project ”PAC-Packaging Attivo Cristallino”.

ACKNOWLEDGMENT

The authors wish to acknowledge Chiesi Farmaceutici S.p.A. for the use of the Bruker D8 Venture single-crystal diffractometer, and the Laboratorio di Strutturistica ‘Mario Nardelli’ of the Dipartimento SCVSA, University of Parma for the diffraction facilities. This work has used resources available from the ‘Department of Excellence’ Project of the Italian MIUR Ministry.

ABBREVIATIONS

AP 4,4’-diazopiridine, F_2AP 3,3’-difluoro-4,4’azopyridine, ClAP 3-chloro-4,4’azopyridine, Cl_2AP 3,3’-dichloro-4,4’azopyridine, Cl_3AP 3,5,3’-trichloro-4,4’azopyridine, Cl_4AP 3,5,3’,5’tetrachloro-4,4’azopyridine,

REFERENCES

(1) Gorman, M. Yogi Berra’s most memorable sayings https://www.newsweek.com/most-memorable-yogi-isms-375661.

(2) Lemmerer, A.; Bernstein, J.; Kahlenberg, V. Covalent Assistance in Supramolecular Synthesis: In Situ Modification and Masking of the Hydrogen Bonding Functionality of the Supramolecular Reagent Isoniazid in Co-Crystals. *CrystEngComm* **2011**, *13*, 5692.

(3) Braga, D.; Grepioni, F.; Maini, L. The Growing World of Crystal Forms. *Chem. Commun.* **2010**, *46*, 6232.

(4) Braun, D. E.; Griesser, U. J. Why Do Hydrates (Solvates) Form in Small Neutral Organic Molecules? Exploring the Crystal Form Landscapes of the Alkaloids Brucine and Strychnine. *Cryst. Growth Des.* **2016**, *16*, 6405–6418.

(5) Harris, R. K.; Ghi, P. Y.; Puschmann, H.; Apperley, D. C.; Griesser, U. J.; Hammond, R. B.; Ma, C.; Roberts, K. J.; Pearce, G. J.; Yates, J. R.; Pickard, C. J. Structural Studies of the Polymorphs of Carbamazepine, Its Dihydrate, and Two Solvates. *Org. Process Res. Dev.* **2005**, *9*, 902–910.

(6) Dunitz, J. D.; Bernstein, J. Disappearing Polymorphs. *Acc. Chem. Res.* **1995**, *28*, 193–200.

(7) Bučar, D.-K.; Lancaster, R. W.; Bernstein, J. Disappearing Polymorphs Revisited. *Angew. Chem. Int. Ed.* **2015**, *54*, 6972–6993.

(8) Javoor, M.; Mondal, P.; Chopra, D. Cocrystals: A Review of Recent Trends in Pharmaceutical and Material Science Applications. *Mater. Sci. Res. India* **2017**, *14*, 09–18.

(9) Almarsson, Ö.; Peterson, M. L.; Zaworotko, M. The A to Z of Pharmaceutical Cocrystals: A Decade of Fast-Moving New Science and Patents. *Pharm. Pat. Anal.* **2012**, *1*, 313–327.

(10) Bolla, G.; Nangia, A. Pharmaceutical Cocrystals: Walking the Talk. *Chem. Commun.*

2016, *52*, 8342–8360.

(11) Braga, D.; Grepioni, F.; Maini, L.; Mazzeo, P. P.; Rubini, K. Solvent-Free Preparation of Co-Crystals of Phenazine and Acridine with Vanillin. *Thermochim. Acta* **2010**, *507–508*, 1–8.

(12) Capucci, D.; Balestri, D.; Mazzeo, P. P.; Pelagatti, P.; Rubini, K.; Bacchi, A. Liquid Nicotine Tamed in Solid Forms by Cocrystallization. *Cryst. Growth Des.* **2017**, *17*, 4958–4964.

(13) Bacchi, A.; Capucci, D.; Giannetto, M.; Mattarozzi, M.; Pelagatti, P.; Rodriguez-Hornedo, N.; Rubini, K.; Sala, A. Turning Liquid Propofol into Solid (without Freezing It): Thermodynamic Characterization of Pharmaceutical Cocrystals Built with a Liquid Drug. *Cryst. Growth Des.* **2016**, *16*, 6547–6555.

(14) Aakeröy, C. B.; Salmon, D. J. Building Co-Crystals with Molecular Sense and Supramolecular Sensibility. *CrystEngComm* **2005**, *7*, 439–448.

(15) Lusi, M. Engineering Crystal Properties through Solid Solutions. **2018**.

(16) Schur, E.; Nauha, E.; Lusi, M.; Bernstein, J. Kitaigorodsky Revisited: Polymorphism and Mixed Crystals of Acridine/Phenazine. *Chem. - A Eur. J.* **2015**, *21*, 1735–1742.

(17) Lusi, M. A Rough Guide to Molecular Solid Solutions: Design, Synthesis and Characterization of Mixed Crystals. *CrystEngComm* **2018**, *20*, 7042–7052.

(18) Mazzeo, P. P.; Carraro, C.; Monica, A.; Capucci, D.; Pelagatti, P.; Bianchi, F.; Agazzi, S.; Careri, M.; Raio, A.; Carta, M.; Menicucci, F.; Belli, M.; Michelozzi, M.; Bacchi, A. Designing a Palette of Cocrystals Based on Essential Oil Constituents for Agricultural

Applications. *ACS Sustain. Chem. Eng.* **2019**, *7*, 17929–17940.

(19) Sheldrick, G. M. SHELXT-Integrated Space-Group and Crystal-Structure Determination. *Acta Cryst A* **2015**, *71*, 3–8.

(20) Sheldrick, G. M. Crystal Structure Refinement with SHELXL. *Acta Cryst. Sec. C* **2015**, *71*, 3–8.

(21) Dolomanov, O. V.; Bourhis, L. J.; Gildea, R. J.; Howard, J. A. K.; Puschmann, H. OLEX2: A Complete Structure Solution, Refinement and Analysis Program. *J. Appl. Crystallogr.* **2009**, *42*, 339–341.

(22) Mackenzie, C. F.; Spackman, P. R.; Jayatilaka, D.; Spackman, M. A. CrystalExplorer Model Energies and Energy Frame-Works: Extension to Metal Coordination Compounds, Organic Salts, Solvates and Open-Shell Systems. **2017**, *4*, 575–587.

(23) Turner, M. J.; McKinnon, J. J.; Wolff, S. K.; Grimwood, D. J. Spackman, P. R. Jayatilaka, D.; Spackman, M. A. CrystalExplorer17. University of Western Australia 2017.

(24) Turner, M. J.; Thomas, S. P.; Shi, M. W.; Jayatilaka, D.; Spackman, M. A. Energy Frameworks: Insights into Interaction Anisotropy and the Mechanical Properties of Molecular Crystals. *Chem. Commun.* **2015**, *51*, 3735–3738.

(25) Thomas, S. P.; Spackman, P. R.; Jayatilaka, D.; Spackman, M. A. Accurate Lattice Energies for Molecular Crystals from Experimental Crystal Structures. **2018**.

(26) Frisch, M. J.; Trucks, G. W.; Schlegel, H. B.; Scuseria, G. E.; Robb, M. A.; Cheeseman, J. R.; Scalmani, G.; Barone, V.; Petersson, G. A.; Nakatsuji, H. et al. Gaussian16 Revision B.01. Gaussian, Inc.: Wallingford CT 2016.

(27) Grimme, S.; Antony, J.; Ehrlich, S.; Krieg, H. A Consistent and Accurate *Ab Initio* Parametrization of Density Functional Dispersion Correction (DFT-D) for the 94 Elements H-Pu. *J. Chem. Phys.* **2010**, *132*, 154104.

(28) Becke, A. D. Density-functional Thermochemistry. III. The Role of Exact Exchange. *J. Chem. Phys.* **1993**, *98*, 5648–5652.

(29) Frisch, M. J.; Pople, J. A.; Binkley, J. S. Self-consistent Molecular Orbital Methods 25. Supplementary Functions for Gaussian Basis Sets. *J. Chem. Phys.* **1984**, *80*, 3265–3269.

(30) Hutchins, K. M.; Kummer, K. A.; Groeneman, R. H.; Reinheimer, E. W.; Sinnwell, M. A.; Swenson, D. C.; MacGillivray, L. R. Thermal Expansion Properties of Three Isostructural Co-Crystals Composed of Isosteric Components: Interplay between Halogen and Hydrogen Bonds. *CrystEngComm* **2016**, *18*, 8354–8357.

(31) Cruz-Cabeza, A. J.; Bernstein, J. Conformational Polymorphism. *Chem. Rev.* **2014**, *114*, 2170–2191.

(32) Hulme, A. T.; Price, S. L.; Tocher, D. A. A New Polymorph of 5-Fluorouracil Found Following Computational Crystal Structure Predictions. *J. Am. Chem. Soc.* **2005**, *127*, 1116–1117.

(33) Heit, Y. N.; Beran, G. J. O. How Important Is Thermal Expansion for Predicting Molecular Crystal Structures and Thermochemistry at Finite Temperatures? *Acta Crystallogr. Sect. B Struct. Sci. Cryst. Eng. Mater.* **2016**, *72*, 514–529.

(34) Kendrick, J.; Montis, R.; Hursthouse, M. B.; Leusen, F. J. J. " *In-Silico* Seeding": Isostructurality and Pseudoisostructurality in a Family of Aspirin Derivatives. *Cryst.*

Growth Des. **2013**, *13*, 2906–2915.

(35) Barnett, S. A.; Hulme, A. T.; Tocher, D. A. 5-Fluorouracil and Thymine Form a Crystalline Solid Solution. **2006**, o4121-0415.

(36) Mariaca, R.; Behrnd, N. R.; Eggli, P.; Stoeckli-Evans, H.; Hulliger, J. Synthesis and Crystal Engineering of Fluorinated Stilbenes. *CrystEngComm* **2006**, *8*, 222–232.

(37) Taga, T.; Yamamoto, N.; Machida, K. Intermolecular Interactions of Fluorine Atoms in the Crystal of l,3-Dimethyl-5-Fluorouracil and Its Mixed Crystal with 1,3-Dimethyluracil. *Bull. Chem. Soc. Jpn.* **1989**, *62*, 354–357.

For Table of Contents Use Only

Diversity through similarity: a world of polymorphs, solid solutions, cocrystals in a vial of 4,4'-diazopyridine

Paolo P. Mazzeo, Claudia Carraro, Anthea Arns, Paolo Pelagatti, Alessia Bacchi

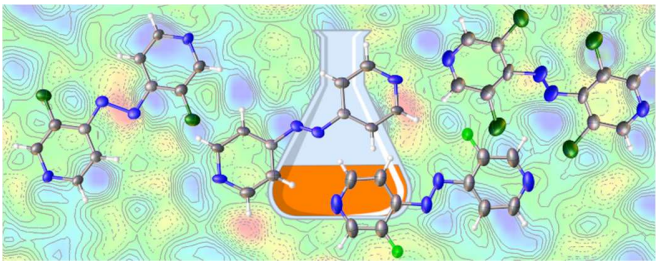

4,4'-diazopyridine and its halogenated derivatives show an amazing propensity to give polymorphs, co-crystals, and solid solutions due to a combination of intermolecular interactions.